Journal of Solid State Chemistry 183 (2010) 1272–1277

Contents lists available at ScienceDirect

Journal of Solid State Chemistry

journal homepage: www.elsevier.com/locate/jssc

Structure and thermal conductivity of $Na_{1-x}Ge_{3+z}$

M. Beekman [a], S. Stefanoski [a], W. Wong-Ng [b], J.A. Kaduk [c], Q. Huang [d], C. Reeg [e], C.R. Bowers [e], G.S. Nolas [a,*]

[a] Department of Physics, University of South Florida, Tampa, FL 33620, USA
[b] Materials Science and Engineering Laboratory, National Institute of Standards and Technology, Gaithersburg, MD 20899, USA
[c] Poly Crystallography, Inc., Naperville, IL 60540, USA
[d] NIST Center for Neutron Research, Gaithersburg, MD 20899, USA
[e] Department of Chemistry, University of Florida, Gainesville, FL 32611, USA

ARTICLE INFO

Article history:
Received 13 January 2010
Received in revised form
25 March 2010
Accepted 27 March 2010
Available online 2 April 2010

Keywords:
Crystal structure
Intermetallic compounds
Thermoelectrics
Thermal conductivity

ABSTRACT

Structural analyses as well as low temperature thermal conductivity is reported for the binary phase $Na_{1-x}Ge_{3+z}$. Specimens were characterized by thermal analysis, conventional and synchrotron powder X-ray diffraction, neutron powder diffraction, ^{23}Na nuclear magnetic resonance spectroscopy, and electrical and thermal transport measurements. With structural characteristics qualitatively analogous to some aluminum-silicate zeolites, the crystal structure of this phase exhibits an unconventional covalently bonded tunnel-like Ge framework, accommodating Na in channels of two different sizes. Observed to be non-stochiometric, $Na_{1-x}Ge_{3+z}$ concurrently exhibits substantial structural disorder in the large channels and a low lattice thermal conductivity, of interest in the context of identifying novel low thermal conductivity intermetallics for thermoelectric applications.

1. Introduction

The science of group 14 elements and the compounds they form is of fundamental importance for development of new or improved materials for many technologically important applications. Binary compounds formed with Ge, particularly with alkali metals, have received attention in a number of respects. There are several known crystalline binary compounds in the Na–Ge system [1]. Of these, Na_4Ge_4 and $Na_{12}Ge_{17}$ have arguably been characterized in the most detail [2–6]. The crystal chemistry of phases such as Na_4Ge_4 and $Na_{12}Ge_{17}$ is well-described in terms of the Zintl–Klemm concepts [7–9]. These compounds are composed of $[Ge_4]^{4-}$ (e.g. Na_4Ge_4 and $Na_{12}Ge_{17}$) or $[Ge_9]^{4-}$ (e.g. $Na_{12}Ge_{17}$) cluster anions and Na^+ cations [2–6]. In Na_4Ge_4, for example, the Na atoms formally transfer their single *s* electron to the Ge polyanion clusters, allowing closed shell configurations for all atoms. The clathrate-II phase Na_xGe_{136} has also been identified, where Na is encapsulated within a Ge cage-like framework at two crystallographic sites with site symmetries $\bar{3}m$ and $4\bar{3}m$ [10,11]. In spite of their simplicity, new and intriguing phases, both thermodynamically stable as well as metastable, continue to be discovered in simple binary systems involving group 14 elements [12–14]. Recently, we discovered the existence of a new binary phase in the Na–Ge system, $Na_{1-x}Ge_{3+z}$ [15]. Here we report on the synthesis, structure, and thermal conductivity of this new binary phase.

2. Synthesis, sample preparation, and experimental methods

One effective route for accessing novel stable and metastable materials is the thermal decomposition of crystalline precursors. The $Na_{1-x}Ge_{3+z}$ phase was prepared by thermal decomposition of the precursor Na_4Ge_4 (monoclinic, space group $P2_1/c$), synthesized by direct reaction of the high purity elements at 650 °C. This reaction was carried out in a tungsten crucible, sealed under ultra high purity nitrogen inside a stainless steel canister, which was in turn sealed inside a fused quartz ampoule. Sodium metal and precursor were handled inside a nitrogen-filled glove box due to the high reactivity of these materials with moisture and air. The $Na_{1-x}Ge_{3+z}$ phase was synthesized by thermal decomposition of coarsely ground Na_4Ge_4 through heating under dynamic vacuum ($\approx 1.33\times10^{-4}$ Pa) at 360 °C for 2 days; results from a systematic investigation into the thermal decomposition of Na_4Ge_4 have been reported previously [11]. During thermal decomposition of Na_4Ge_4 under dynamic vacuum, Na is evolved as vapor. Amorphous and moisture sensitive solids of unknown constitution are typically present in the as-synthesized specimens. While the amorphous by-products apparently have a low solubility in water, they can be readily separated from the crystalline fraction

* Corresponding author.
E-mail addresses: gnolas@cas.usf.edu, gnolas@chuma1.cas.usf.edu (G.S. Nolas).

0022-4596/$ - see front matter © 2010 Elsevier Inc. All rights reserved.
doi:10.1016/j.jssc.2010.03.035

by repeated brief sonication in distilled water followed by immediate decanting of the resulting impurity-containing suspension, leaving single phase crystalline $Na_{1-x}Ge_{3+z}$ product, which more quickly settles to the bottom of the container. The product is then rinsed with ethanol and dried. The remaining products from this process were greyish microcrystalline powders that were stable in air and moisture and free from amorphous by-products. The stability toward moisture of $Na_{1-x}Ge_{3+x}$ relative to Na_4Ge_4 is related to the presence of Na^+ cations and $[Ge_4]^{4-}$ polyanions in Na_4Ge_4, as compared to Na^+ and a three-dimensional covalently bonded Ge-framework in $Na_{1-x}Ge_{3+z}$ (discussed below). These observations are analogous to the stability of alkali-tetralide clathrates [14].

Fig. 1 shows data from differential thermal analysis acquired under flowing nitrogen in open alumina pans, at the heating rate of 20 °C/min. The thermal analysis measurements revealed decomposition of the title phase commences exothermically above 400 °C under these conditions (inset), whereas decomposition begins under vacuum (10^{-4} Pa) at the slightly lower temperature of 370 °C [11]. The exothermic nature of the decomposition suggests the phase is thermodynamically metastable with respect to the constituent elements under the conditions described above.

Two different specimens prepared from two different syntheses were used for synchrotron X-ray and neutron powder diffraction experiments, respectively. Synchrotron X-ray powder diffraction data (Specimen I) were collected on the 32ID beamline of the Advanced Photon Source at Argonne National Laboratory (APS) and neutron powder diffraction intensity data (Specimen II) were collected using the BT-1 high-resolution powder diffractometer at the National Institute for Standards and Technology Center for Neutron Research; further details can be found in Ref. [15]. Conventional powder X-ray diffraction (PXRD) data were collected using Cu$K\alpha$ radiation.

The solid-state ^{23}Na magic angle spinning (MAS) nuclear magnetic resonance (NMR) spectrum of the microcrystalline powder sample was acquired at room temperature with a Bruker Avance 400 MHz spectrometer (ν_0=105.841 MHz) in a 4 mm outer diameter ZrO_2 rotor, in a Bruker multinuclear MAS probe head. The sample was spun at 8.8 kHz, and the single pulse-acquisition sequence was employed using a pulse length of 1.0 μs with an RF field of 100 kHz.

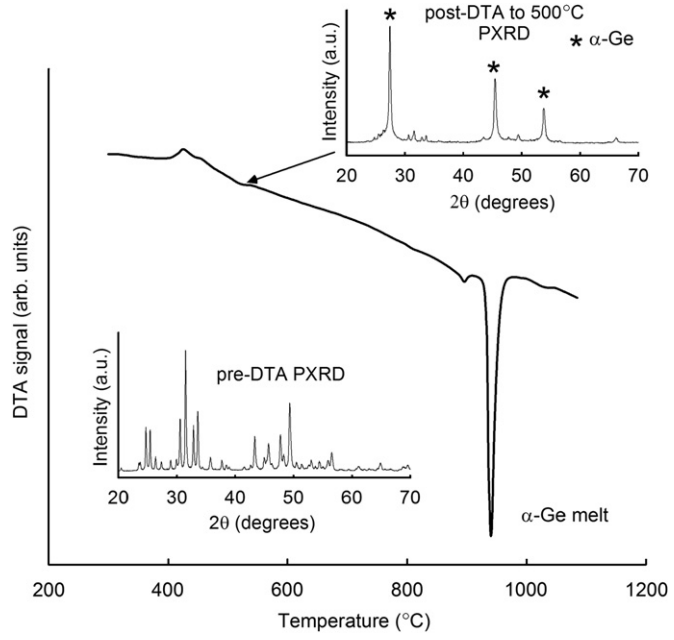

Fig. 1. Differential thermal analysis (DTA) data (exothermic up) for $Na_{1-x}Ge_{3+z}$, indicating decomposition near 400 °C. The prominent endothermic event at ≈940 °C corresponds to the melting of α-Ge. Lower left: pre-DTA PXRD pattern. Upper right: post-DTA PXRD pattern for a portion of the sample after DTA to 500 °C, indicating decomposition products contain α-Ge as the majority phase, with trace amounts of the title phase remaining.

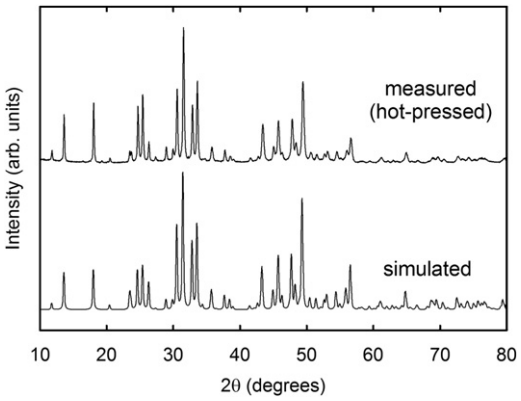

Fig. 2. Simulated PXRD pattern (bottom) for $Na_{1-x}Ge_{3+z}$, based on the structural model obtained from neutron diffraction at 295 K, along with PXRD pattern from the $Na_{1-x}Ge_{3+z}$ specimen collected after hot-pressing.

To investigate the thermal conductivity of $Na_{1-x}Ge_{3+z}$, a consolidated specimen was prepared by hot-pressing. Achieving high relative densities in the compact was found to be challenging, due to the metastable nature of the phase (Fig. 1) which precluded the use of high sintering temperatures typically needed to produce a pellet of relatively high density. A pellet exhibiting 65% of the expected (diffraction) density was obtained by hot-pressing at 250 °C, and 130 MPa for 1 h. The PXRD pattern obtained after hot-pressing, shown in Fig. 2, confirmed that the crystallinity of the specimen was maintained and decomposition did not occur during consolidation. No preferred orientation of the crystallites in the consolidated pellet was observed. Room temperature Seebeck coefficient and electrical resistivity, and temperature dependent thermal conductivity were then investigated on parallelepipeds sectioned from the pellet using a diamond saw.

3. Crystal structure of $Na_{1-x}Ge_{3+z}$

The space group was determined to be $P6/m$ (no. 175) from initial synchrotron diffraction and confirmed by neutron diffraction [15]. Refinement results, refined hexagonal unit cell parameters, and refined compositions are given in Table 1. The crystal structure determined from synchrotron experiments was confirmed and the structural model was refined against neutron diffraction data at 295 and 4 K. Crystallographic data for $Na_{1-x}Ge_{3+z}$ obtained from Rietveld refinement against synchrotron X-ray and neutron powder diffraction are given in Tables 2 and 3.

$Na_{1-x}Ge_{3+z}$ exhibits a unusual zeolite-like framework structure. A depiction of the crystal structure as determined from neutron diffraction is shown in Fig. 3. The most conspicuous aspect of the crystal structure is a covalently bonded framework of Ge atoms, all of which are arranged in distorted tetrahedral (i.e. 4-bonded) configurations with the exception of Ge1, which is only bonded to three other Ge atoms. The framework forms large and small channels along the c-direction, akin to the channels found in some oxide zeolites (cf. qualitative structural similarities to the AFI aluminum phosphate zeolite type [16]); however, to our

Table 1
Crystal structure refinement results for Specimens I (synchrotron X-ray powder diffraction) and II (neutron powder diffraction).

	Specimen I (synchrotron)	Specimen II (neutron)	
		295 K	4 K
R values			
wR_p	0.0445	0.0204	0.0213
R_p	0.0257	0.0171	0.0178
χ^2	2.164	1.195	1.46
No. of variables	28	57	57
Total # data points	40,699	3119	3120
Impurity phases	Amorphous	Ge (1.2%)	Ge (1.2%)
Cell parameters			
a (Å)	15.05399(5)	15.0640(3)	15.0052(4)
c (Å)	3.96845(2)	3.9673(1)	3.9546(1)
V (Å^3)	778.852(5)	779.66(3)	771.10(4)
Refined composition	$Na_{0.71}Ge_{3.08}$	$NaGe_{3.25}$	$NaGe_{3.24}$

Table 2
Crystallographic data for $Na_{1-x}Ge_{3+z}$ from Rietveld refinement against synchrotron X-ray (Specimen I) and neutron powder diffraction (Specimen II).

Atom	Wyckoff position	*x*	*y*	*z*	U_{iso} or U_{eq} (Å^2)	Occupancy
Synchrotron X-ray *data* (*Specimen I*)						
Ge1	6*j*	0.37332(8)	0.26958(8)	0	0.0115(4)	1
Ge2	6*j*	0.40826(8)	0.44914(8)	0	0.0106(4)	1
Ge3	6*k*	0.52012(9)	0.15164(9)	1/2	0.0052(3)	1
Ge4	6*k*	0.48411(10)	0.30138(7)	1/2	0.0071(3)	1
Na5	2*c*	2/3	1/3	0	0.02	1
Na6	6*k*	0.2539(6)	0.0639(7)	1/2	0.088(4)	0.617(9)
Ge7	1*b*	0	0	1/2	0.088	0.617(9)
Neutron diffraction data at 295 K[a] (*Specimen II*)						
Ge1	6*j*	0.3689(3)	0.2666(3)	0	0.0108(4)	1
Ge2	6*j*	0.4069(3)	0.4482(3)	0	0.0108(4)	1
Ge3	6*k*	0.5186(3)	0.1518(4)	1/2	0.0108(4)	1
Ge4	6*k*	0.4842(4)	0.2996(3)	1/2	0.0108(4)	1
Na5	2*c*	2/3	1/3	0	0.038(5)	1
Na6	6*k*	0.260(1)	0.068(1)	1/2	0.08534	1
Ge7	12*l*	0.108(2)	0.029(3)	0.140(5)	0.052(7)	0.163(4)
Neutron diffraction data at 4 K[b] (*Specimen II*)						
Ge1	6*j*	0.3674(3)	0.2652(3)	0	0.0054(4)	1
Ge2	6*j*	0.4058(3)	0.4479(3)	0	0.0054(4)	1
Ge3	6*k*	0.5180(3)	0.1510(3)	1/2	0.0054(4)	1
Ge4	6*k*	0.4842(3)	0.2996(3)	1/2	0.0054(4)	1
Na5	2*c*	2/3	1/3	0	0.01956	1
Na6	6*k*	0.259(1)	0.0701(9)	1/2	0.07499	1
Ge7	12*l*	0.112(2)	0.034(2)	0.141(4)	0.033(5)	0.16667

[a] Anisotropic displacement parameters for Na5 and Na6 in the order of U_{11}, U_{22}, U_{33}, U_{12}, U_{13}, U_{23} are 0.045(8), 0.045(8), 0.02(1), 0.023(4), 0, 0; and 0.10(1), 0.05(1), 0.08(1), 0.02(1), respectively.

[b] Anisotropic displacement parameters for Na5 and Na6 in the order of U_{11}, U_{22}, U_{33}, U_{12}, U_{13}, U_{23} are 0.023(5), 0.023(5), 0.012(8), 0.012(2), 0, 0; and 0.11(1), 0.094(5), 0.049(7), −0.016(7), respectively.

knowledge $Na_{1-x}Ge_{3+z}$ does not correspond to any of the known zeolite structure types [16]. The four crystallographically independent Ge framework sites (Ge1, Ge2, Ge3, and Ge4; cf. Table 2) were all found to be fully occupied in refinements against both synchrotron and neutron diffraction data. From neutron diffraction at 295 K, the Ge–Ge distances in the framework (cf. Table 3) range from 2.438(8) to 2.527(6) Å, as compared to the known bond length of 2.45 Å for elemental Ge in the diamond structure (α-Ge) [17]. The open-framework configuration of Ge in $Na_{1-x}Ge_{3+z}$ results in an unusually large volume per Ge atom of nearly 33 Å^3/atom. This can be compared to 23 Å^3/atom for α-Ge and 26 Å^3/atom for the guest-free clathrate-II Ge_{136} [18], and indicates the pronounced "openness" of the Ge framework in $Na_{1-x}Ge_{3+z}$.

The covalent Ge framework of $Na_{1-x}Ge_{3+z}$ differs from the polyanionic $[Ge_4]^{4-}$ or $[Ge_9]^{4-}$ cluster units found in other Na–Ge compounds such as Na_4Ge_4 and $Na_{12}Ge_{17}$ [2–6]. Fig. 3b shows two perspectives of the small and large framework channels in the structure. Na atoms are situated inside the small channels (Na5), as well as in the broad channels (Na6). The broad channel consists of alternating Ge and Na; the Ge forming this channel may also be described as a 24-ring. A maximum of six Na atoms can occupy the Na6 sites inside the broad channels that are related to each other by 6-fold symmetry. The initial synchrotron experiments and corresponding structure refinements suggested that Ge atoms are disordered in the middle of the broad channel in Specimen I. In refinements against neutron diffraction data collected at both 295 and 4 K, the nuclear density in the broad channel could be

Table 3
Selected interatomic distances for $Na_{1-x}Ge_{3+z}$.

Atom–atom	Specimen 1	Specimen II	
	295 K (synchrotron)	295 K (neutron)	4 K (neutron)
(i) Ge–Ge bonds (Å)			
Ge1–Ge2	2.482(1)	2.499(5)	2.504(4)
Ge1–Ge4	2.4798(9) × 2	2.516(4) × 2	2.519(3) × 2
Ge2–Ge1	2.482(1)	2.499(5)	2.504(4)
Ge2–Ge2	2.397(2)	2.438(8)	2.453(7)
Ge2–Ge3	2.465(1) × 2	2.463(4) × 2	2.443(3) × 2
Ge3–Ge2	2.456(1) × 2	2.463(4) × 2	2.443(3) × 2
Ge3–Ge4	2.569(1)	2.526(7)	2.522(6)
Ge3–Ge4	2.486(2)	2.527(6)	2.523(6)
Ge4–Ge1	2.4798(9) × 2	2.516(4) × 2	2.519(3) × 2
Ge4–Ge3	2.569(1)	2.526(7)	2.522(6)
Ge4–Ge3	2.486(2)	2.527(6)	2.523(6)
(ii) Na–Ge and Na–Na distances (Å)			
Na5–Ge3	3.202(1) × 6	3.206(4) × 6	3.205(3) × 6
Na5–Ge4	3.225(1) × 6	3.218(4) × 6	3.205(3) × 6
Na5–Na5	3.96845(1) × 2	3.9673(1) × 2	3.9546(1) × 2
Na6–Ge1	3.457(7) × 2	3.27(1) × 2	3.22(1) × 2
Na6–Ge1	3.310(7) × 2	3.29(1) × 2	3.29(1) × 2
Na6–Ge3	3.537(7) × 2	3.45(2) × 2	3.44(2) × 2
Na6–Ge4	3.522(8) × 2	3.44(2) × 2	3.41(1) × 2
Na6–Na6	3.96845(1) × 2	3.9673(1) × 2	3.95455(1) × 2
Na6–Na6	3.444(7) × 2	3.51(2) × 2	3.48(2) × 2
Na6–Ge7	3.447(7)	2.50(3) × 2	2.44(1) × 2
		3.26(2) × 2	3.22(2) × 2
		3.38(4)	3.39(3)
		3.37(4) × 2	3.30(3) × 2

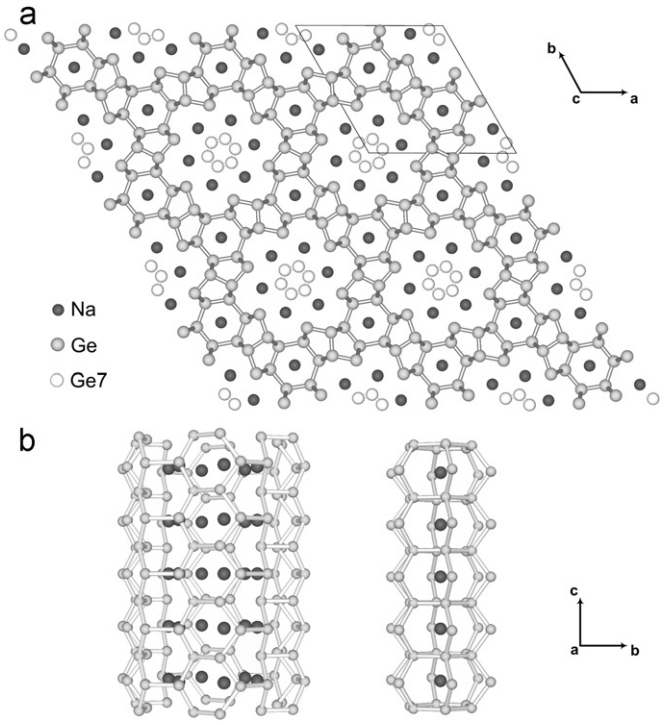

Fig. 3. (a) Depiction of the crystal structure of $Na_{1-x}Ge_{3+z}$ viewed down the *c*-axis. (b) Depiction of the two channels as viewed down the *a*-axis. At left is the large channel, at right is the smaller channel, where Na are coordinated in an 18-membered Ge cage.

modeled by assigning Ge to disordered sites near the center of the broad channel in Specimen II. In both cases, these extra-framework Ge sites were not found to be fully occupied, in contrast to the connected Ge framework. The Ge7 site in Specimen II was found to have occupancy of 1/6 suggesting the Ge atoms in this case may be disordered on one Ge7 site per larger channel, per layer progressing along the *c*-axis. It was observed that the content of both species in the larger channel (Ge7 and Na6) can vary depending on the synthesis conditions. In particular, repeated grinding under nitrogen atmosphere and then "degassing" (i.e. further heating the $Na_{1-x}Ge_{3+z}$ specimen under vacuum at 350 °C) was found to reduce the Na content in the larger channel (cf. Specimen I). This suggests a significant mobility of Na in the larger channel facilitating removal from the structure when heated under vacuum, analogous to behavior observed in the Na_xSi_{136} clathrates [19]. From our synchrotron X-ray and neutron diffraction studies on the two different specimens, the Ge content inside the broad channel (Ge7 positions) appears to be variable as well. With the Ge framework, Na5, and Na6 sites all fully occupied, the chemical formula of this new phase would be $NaGe_3$. However, since the Na6 and Ge7 occupancies inside the larger channel can vary, the phase is non-stoichiometric with general formula $Na_{1-x}Ge_{3+z}$. Considering the refined compositions from Specimen I ($Na_{0.71}Ge_{3.08}$) and Specimen II ($NaGe_{3.25}$), we can infer a significant phase width of at least 5 at% Na for this metastable phase.

Examination of the anisotropic atomic displacement parameters (U_{ij}; cf. Table 2) for Na6 in the larger channel reveals significant disorder. A pronounced cigar-like elongation of the Na6 displacement ellipsoid indicates substantial disorder for this site, and suggests the structural model only approximates this disorder in the large channel. Moreover, the U_{11} element of the U_{ij} tensor remains very large even at 4 K. At the same time, U_{22} and U_{33} both exhibit rather large values and stronger temperature dependence, indicating significant thermal motion for Na6 as well. This static and thermal disorder suggested by U_{ij} for this site can be understood in terms of the rather poor bonding environment of the large channel, as well as the presence or absence of the nearby Ge7 in its fractionally occupied site.

The ^{23}Na MAS NMR spectrum, referenced to 1 M NaCl at 0×10^{-6}, is shown in Fig. 4. A broad manifold of spinning sidebands is observed in Fig. 4a, from which a quadrupole coupling constant of $e^2qQ/h \approx 350$ kHz and an asymmetry parameter of $\eta = 0$ are estimated. The expansion in Fig. 4b reveals two distinct peaks, centered at 4×10^{-6} and 23×10^{-6}, consistent with the two crystallographic environments for Na (Na5 and Na6 above) in $Na_{1-x}Ge_{3+z}$. The magnitudes of the shifts are relatively small (i.e. the resonances are close to that for Na^+ in NaCl), suggesting that both Na are in an essentially ionic state in this phase. Large ^{23}Na paramagnetic and/or Knight shifts (ca. $1600–2000 \times 10^{-6}$) that have been observed for the Na_xSi_{136} clathrates are not observed in $Na_{1-x}Ge_{3+z}$ [19,20]. The sideband pattern is associated with the central transition at 4×10^{-6}, which upon closer inspection (Fig. 4b), reveals at least three overlapping transitions. The T_1 relaxation time of this peak and its sidebands is approximately 1 s. The large peak at 23×10^{-6}, which does not exhibit sidebands or any direct evidence of a quadrupole coupling, has a much shorter relaxation time of $T_1 < 20$ ms, as determined by progressive saturation. Since the integrated NMR peak area is proportional to the multiplicity of the site in the crystal structure, we can assign the peak with higher intensity at approximately 23×10^{-6} to Na in the larger channel (multiplicity of 6) and the peak with lower intensity at approximately 4×10^{-6} to Na in the smaller channel (multiplicity of 2). This assignment is also consistent with the much shorter relaxation time and absence of spinning sidebands due to molecular motion in the large channels, in agreement with the neutron diffraction data presented above. The relative peak areas are consistent with the 3:1 site multiplicity. It would appear that the satellite transitions of the Na6 nuclei do not significantly contribute to the area of the peak at 23×10^{-6}.

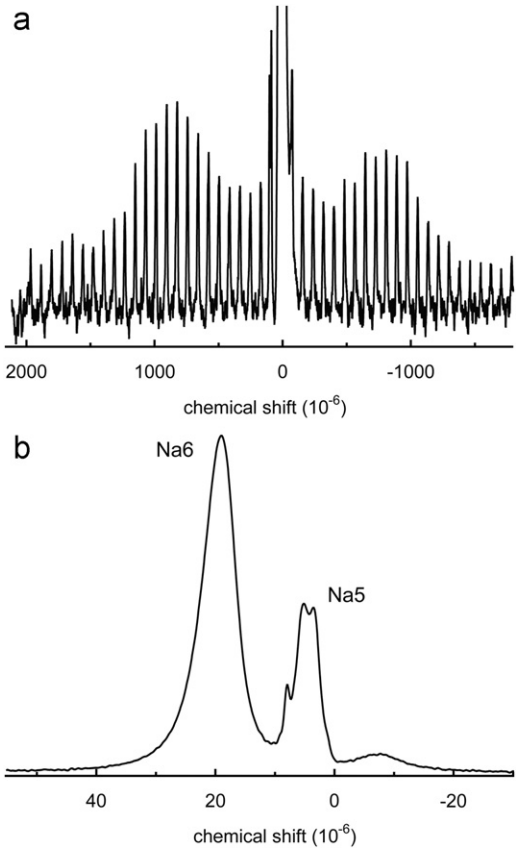

Fig. 4. Solid-state ^{23}Na magic angle spinning NMR data for $Na_{1-x}Ge_{3+z}$. The spectrum is referenced to 1 M NaCl at 0×10^{-6}: (a) vertical expansion to show the spinning sidebands and (b) horizontal expansion of the central transition region.

4. Transport properties of $Na_{1-x}Ge_{3+z}$

Room temperature Seebeck (S) measurements yielded the value $-330\,\mu V/K$. This relatively large magnitude for the Seebeck coefficient is comparable to values for undoped compound semiconductors [21]. Although we were unable to obtain a reliable room temperature electrical resistivity value for the specimen due to difficulties in achieving adequate electrical contacts and the large electrical resistance of the specimen, our measurements indicate a large resistivity of the order $10^5\,m\Omega\,cm$. This large apparent resistivity likely originates from the low relative density achieved during consolidation.

Fig. 5 shows the thermal conductivity, κ, of the $Na_{1-x}Ge_{3+z}$ specimen in the temperature range from 12 to 300 K. As a result of the complex hexagonal crystal structure of $Na_{1-x}Ge_{3+z}$, the transport properties are likely anisotropic and therefore the data obtained from the polycrystalline specimen should be interpreted as some average measure of the transport in the different crystallographic directions. Also shown in Fig. 5 are the thermal conductivities for single crystal α-Ge [22], clathrate-I K_8Ge_{44} [23], as well as for polycrystalline and amorphous Ge films [24]. Since the porosity of the $Na_{1-x}Ge_{3+z}$ specimen was considerable (~35%), the data shown in Fig. 5 have been corrected accordingly. It is known that porosity in polycrystalline specimens can significantly reduce the observed κ [25–28]. Methods have been developed in order to account for these effects [25–28], with particularly valuable discussions on the effects of porosity on κ of solids given by Klemens et al. [27,28]. As detailed in Ref. [27], the thermal conductivity of the "fully dense" material, κ_{dense}, can be estimated from the observed κ of a porous specimen, κ_{porous}, using the relation $\kappa_{porous}/\kappa_{dense} = 1-3\varphi/2$,

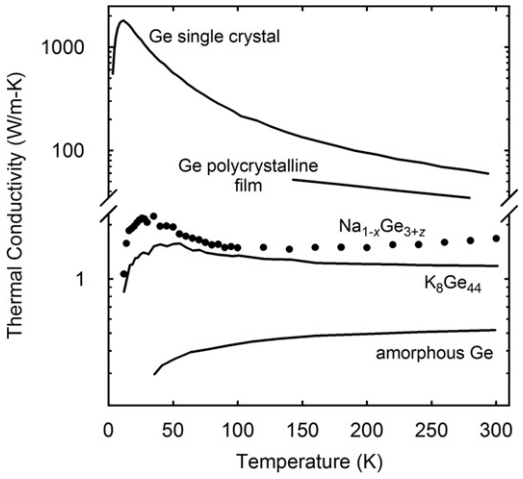

Fig. 5. Thermal conductivity of $Na_{1-x}Ge_{3+z}$. Also shown are the thermal conductivities of bulk single-crystal Ge [22], clathrate-I K_8Ge_{44} [23], as well as polycrystalline and amorphous Ge films [24].

where φ is the relative porosity in the porous specimen. This approach was shown to be successful in modeling the effects of porosity on κ of yttrium stabilized zirconia [28]. The data for $Na_{1-x}Ge_{3+z}$ in Fig. 5 are the adjusted data using this approach. The κ_{dense} values of $Na_{1-x}Ge_{3+z}$ are found to be very low, near $1.4\,W\,m^{-1}\,K^{-1}$ in the temperature range investigated. From the large room temperature resistivity, we can infer that the electronic contribution to κ is negligible, and thus the observed κ of $Na_{1-x}Ge_{3+z}$ can be attributed almost entirely to the lattice component.

As the bonding in the Ge framework of $Na_{1-x}Ge_{3+z}$ is similar to that in α-Ge, it is useful to compare with the thermal conductivities shown in Fig. 5 for other elemental forms and a binary clathrate compound of K and Ge. κ of the $Na_{1-x}Ge_{3+z}$ phase is quite low as compared to single or polycrystalline Ge, approaching that of amorphous Ge in magnitude and similar to the clathrate-I phase K_8Ge_{44}. We attribute the low κ values of this material to the unusual features of its unique crystal structure. Low thermal conductivities typically observed [29,30] for the structurally analogous oxide zeolites have been attributed to the openness of their framework crystal structures, as well as contributions (e.g. point-defect and resonant scattering) from extra-framework species residing in the tunnels and cages in these structures [30]. The structural analysis above and our observation of very low κ for $Na_{1-x}Ge_{3+z}$ suggest that these factors likely also impede thermal transport in non-oxide, intermetallic materials with similar structural architectures. Pronounced static disorder and thermal motion present in the large channel of the crystal structure, combined with the relatively large number of atoms in the unit cell, may play a significant role in impeding heat transport in $Na_{1-x}Ge_{3+z}$.

5. Conclusions

$Na_{1-x}Ge_{3+z}$ constitutes the first example in which an exclusively germanium framework crystallizes in a tunnel configuration, reminiscent of those found in the microporous oxide zeolites but here obtained in an intermetallic system. An intermetallic compound with some structural similarities to our material, the orthorhombic phase Na_5Sn_{13} with covalently bonded Sn atoms and Na atoms occupying two different channels in the structure, has been reported by Vaughney and Corbett [31]. The existence of these two phases exemplifies that novel and complex structural

architectures can be obtained in simple binary systems between the alkali and group 14 elements. Although the large resistivity of the composition reported on here results in relatively low room temperature thermoelectric performance for these specimens, the low κ observed for $Na_{1-x}Ge_{3+z}$ indicates the structural features of open-framework intermetallic compounds could be favorable in searching for new thermoelectric materials. Moreover, the non-stoichiometry and phase width implied by the synchrotron X-ray and neutron powder diffraction experiments above suggests that the composition of $Na_{1-x}Ge_{3+z}$ can be varied. It is therefore of interest for future study to determine if the physical properties, and in particular the electrical properties, can in turn be systematically influenced by varying the composition of this intriguing material.

Acknowledgments

M.B., S.S. and G.S.N. acknowledge support from US DOE Grant no. DE-FG02-04ER46145. M.B. acknowledges support from the USF Presidential Doctoral Fellowship. Figs. 2 and 3 were created with the aid of the software PowderCell [32] and Balls & Sticks [33], respectively. GSAS [34] and EXPGUI [35] software were used for Rietveld structure refinements.

Appendix A. Supplemental data

Supplementary data associated with this article can be found in the online version at doi:10.1016/j.jssc.2010.03.035.

References

[1] J. Sangster, A.D. Pelton, J. Phase Equilibria 18 (1997) 295–297.
[2] J. Witte, H.G. von Schnering, Z. Anorg. Allg. Chem. 327 (1964) 260–273.
[3] R. Schäfer, W. Klemm, Z. Anorg. Allg. Chem. 312 (1961) 214–220.
[4] H.G. von Schnering, M. Baitinger, U. Bolle, W. Carrillo-Cabrera, J. Curda Y. Grin, F. Heinemann, J. Llanos, K. Peters, A. Schmeding, M. Somer, Z. Anorg. Allg. Chem. 623 (1997) 1037–1039.
[5] C. Hoch, M. Wendorff, C. Röhr, J. Alloys Compd. 361 (2003) 206–221.
[6] W. Carrillo-Cabrera, R.C. Gil, M. Somer, Ö. Persil, H.G. von Schnering, Z. Anorg. Allg. Chem. 629 (2003) 601–608.
[7] E. Zintl, Angew. Chem. 52 (1939) 1–6.
[8] W. Klemm, E. Busmann, Z. Anorg. Allg. Chem. 319 (1963) 297–311.
[9] S.M. Kauzlarich (Ed.), Chemistry, Structure and Bonding of Zintl Phases and Ions, VCH, New York, 1996.
[10] C. Cros, M. Pouchard, P. Hagenmuller, J. Solid State Chem. 2 (1970) 570–581.
[11] M. Beekman, J. Gryko, H.F. Rubin, J.A. Kaduk, W. Wong-Ng, G.S. Nolas, in: Proceedings of the 24th International Conference on Thermoelectrics, IEEE catalog #05TH8854, Piscataway, NJ, 2005, pp. 234–237.
[12] P.H. Tobash, S. Bobev, J. Solid State Chem. 180 (2007) 1575–1581.
[13] A.M. Guloy, Z. Tang, R. Ramlau, B. Böhme, M. Baitinger, Y. Grin, Eur. J. Inorg. Chem. 17 (2009) 2455–2458.
[14] M. Beekman, M. Baitinger, H. Borrmann, W. Schnelle, K. Meier, G.S. Nolas, Y Grin, J. Am. Chem. Soc. 131 (2009) 9642–9643.
[15] M. Beekman, J.A. Kaduk, Q. Huang, W. Wong-Ng, W. Yang, D. Wang G.S. Nolas, Chem. Commun. 1 (2007) 837–839.
[16] C. Baerlocher, L.B. McCusker, Database of zeolite structures, available at ⟨http://www.iza-structure.org/databases/⟩.
[17] N.A. Goryunova, The Chemistry of Diamond-like Semiconductors, Chapman Hall, London, 1965.
[18] A.M. Guloy, R. Ramlau, Z. Tang, W. Schnelle, M. Baitinger, Y Grin, Nature 443 (2006) 320–323.
[19] M. Beekman, G.S. Nolas, J. Mater. Chem. 18 (2008) 842–851.
[20] J. Gryko, P.F. McMillan, R.F. Marzke, A.P. Dodokin, A.A. Demkov, O.F. Sankey, Phys. Rev. B 57 (1998) 4172–4179.
[21] A.F. Ioffe, The Physics of Semiconductors, Academic Press, New York, 1960.
[22] C.J. Glassbrenner, G.A. Slack, Phys. Rev. 134 (1964) A1058–A1069.
[23] M. Beekman, G.S. Nolas, Int. J. Appl. Ceram. Technol. 4 (2007) 332–338.
[24] D.G. Cahill, H.E. Fischer, T. Klitsner, E.T. Swartz, R.O. Pohl, J. Vac. Sci. Technol. A 7 (1989) 1259–1266.
[25] S.L. Loeb, J. Am. Ceram. Soc. 37 (1954) 96–99.
[26] J. Francl, W.D. Kingery, J. Am. Ceram. Soc. 37 (1954) 99–107.
[27] P.G. Klemens, High Temp.-High Pressures 23 (1991) 241–248.
[28] K.W. Schlichting, N.P. Padture, P.G. Klemens, J. Mater. Sci. 36 (2001) 3003–3010.
[29] V.V. Murashov, M.A. White, Mater. Chem. Phys. 75 (2002) 178–180.
[30] V.V. Murashov, J. Phys.: Cond. Matter 11 (1999) 1261–1271.
[31] J.T. Vaughney, J.D. Corbett, Inorg. Chem. 36 (1997) 4316–4320.
[32] W. Kraus, G. Nolze, J. Appl. Crystallogr. 29 (1996) 301.
[33] T.C. Ozawa, S.J. Kang, J. Appl. Crystallogr. 37 (2004) 679.
[34] A.C. Larson, R.B. Von Dreele, General structure analysis system (GSAS), Los Alamos National Laboratory Report LAUR 86-748, 2004.
[35] B.H. Toby, J. Appl. Crystallogr. 34 (2001) 210.